SSRG International Journal of Electronics and Communication Engineering
ISSN: 2348-8549/ https://doi.org/10.14445/23488549/IJECE-V13I8P107

Volume 13 Issue 8, 99-112, August 2026

Original Article

Transient Stability Assessment of a Grid-Connected Micro-Hydro Power Plant Using MATLAB/Simulink Under Multiple Fault Conditions with Controller Performance Analysis

Pooja Shashikant Bansode[1], Swapnil Yashavant Gadgune[2], Sushant Subhash Kamble[3], Ambadas B. Shinde[4]

[1,2]*Department of Electrical Engineering, Padmabhooshan Vasantraodada Patil Institute of Technology, Budhgaon, Sangli, Maharashtra, India.*
[3]*Department of Electrical Engineering, Walchand College of Engineering, Sangli, Maharashtra, India.*
[4]*Department of Electronics and Computer Science Engineering, P. V. P. Institute of Technology, Sangli, Maharashtra, India.*

[2]*Corresponding Author : swapnilgadgune.ele@pvpitsangli.edu.in*

Received: 10 April 2026 Revised: 02 June 2026 Accepted: 30 July 2026 Published: 31 August 2026

Abstract - *The issue of transient stability demands careful attention when integrating micro-hydro power plants into the utility grid, since synchronous generating units of small capacity are highly sensitive to electrical disturbances, particularly short-circuit faults of varying severity. Rigorous dynamic modeling is therefore essential to capture the coupled interactions among the hydraulic, electrical, and control subsystems under disturbed operating conditions. This paper develops a MATLAB/Simulink-based transient stability model of a grid-connected run-of-river micro-hydro power plant comprising a hydraulic turbine-governor, a synchronous generator, an automatic voltage regulator and excitation system, a step-up transformer, connected loads, and an infinite-bus grid, rated at 100 kVA, 11 kV, 50 Hz. The system is subjected to four distinct fault types, namely a Symmetrical Three-Phase-to-Ground (3LG) fault, a Single Line-to-Ground (SLG) fault, a Line-to-Line (LL) fault, and a double Line-to-Ground (LLG) fault, each applied at 0.1 s and cleared at 0.2 s, together with a parametric study covering different fault-clearing times and load variation conditions. Terminal voltage, rotor speed, stator current, and field voltage are analyzed across all scenarios. In addition, a comparative evaluation of controller performance is carried out, contrasting the conventional governor and IEEE Type-1 AVR configuration with an optimized PID governor and a fuzzy-logic-based excitation controller. The results demonstrate that synchronism is maintained across all fault types and operating conditions. The comparative controller analysis confirms that optimized and intelligent control strategies reduce post-fault settling time by approximately 45% relative to the conventional baseline. The findings establish the presented framework as a reliable basis for fault-type-dependent stability assessment, controller benchmarking, and grid-integration planning of micro-hydro generation systems.*

Keywords - *Micro-hydropower, Grid integration, Transient stability, MATLAB/Simulink, Synchronous generator, Asymmetrical faults, Controller comparison, Fault-clearing time.*

1. Introduction

The ongoing change of the energy system to cleaner models, no longer grounded in traditional fossil-fuel-based generation, has further boosted the need on renewable sources that are not only sustainable, but also technically compatible with the current power networks [1].

In this shift, distributed renewable generation has become especially significant due to its potential to enhance local energy access, decrease transmission reliance, and assist in decarbonization goals [2]. Micro-hydropower has a special niche among the distributed renewable options, as it is based on a well-established conversion principle, offers a more predictable primary energy source compared to intermittent ones, and can be located in geographically appropriate locations to accomplish both rural electrification and grid connection [3]. The increasing integration of these small-scale renewable systems into power systems, however, also shifts the focus of the research to dynamic performance, controllability and system stability under disturbed operating conditions [4].Micro-hydropower is particularly attractive in run-of-river projects, whereby generation of electricity can be achieved without huge reservoirs, and a comparatively smaller ecological footprint can be achieved [5]. It can be applied to the distributed generation research and to the grid-support practice [6] due to its applicability to remote areas and semi-urban conditions and its comparatively high level of utilization. Water contribution to a micro-hydro plant is typically much more continuous than highly intermittent renewable sources, and this allows the generation unit to be more continuously operated both in the short and medium term [7]. This feature makes micro-hydro a good candidate for local grid support, support in voltage regulation, and stable integration of renewable. At the same time, with interconnection with an adequate utility grid, the size of such systems relative to the network cannot nullify dynamic problems; in fact, it only increases the importance of modeling and control in this case, as a small generating unit must be able to stay in step and operational when subjected to extreme electrical disturbances [8, 9].

The technical challenge is amplified when grid-connected micro-hydro plants are subjected to transient disturbances like sudden changes in load, short-circuit faults and network-side voltage depressions [10]. The relationship between mechanical input power and electrical output power is broken in such events and results in electromechanical oscillations, which may take the form of rotor speed deviation, current bursts, and voltage collapse or recovery pulses [11]. These upsets are directly connected with the hydraulic and electrical subsystems in a micro-hydro system based on a synchronous generator. The governor must respond to speed error by changing turbine input by adjusting water flow and gate position, and the excitation system must respond to changes in field voltage to maintain generator terminal voltage. In this way, the concerted effort of the turbine-governor loop and the automatic voltage regulator is the center of attention in the provision of reasonable dynamic operation and the removal of instability following a disturbance [12, 13].

The existing literature on the subject of micro-hydro systems could be divided into three related groups rather loosely. The first cluster deals with the overall modeling of micro-hydro plants and highlights the necessity of modeling turbine, generator, and network interactions within a unified simulation framework [14]. The second group centers around the control layer, especially speed governor and excitation control, acknowledging that the behavior of frequency, voltage, and active power in small hydro units is highly dependent on the design and tuning of these controllers [15].

The third cluster examines transient behavior under faulted or disturbed conditions, in which the primary issue is whether the generating unit can regain synchronism, re-establish voltage, and restrain excessive current following disturbance clearance [16]. These themes are also indicated in the literature reviewed in the first-phase report of the project, including previous studies on micro-hydro generation controls and performance analysis under conditions of instability in a power system, as well as more general considerations of distributed renewable integration and the applicability of small hydro.

Even with these contributions, a significant gap exists between general conceptual arguments of micro-hydro integration and time-domain analysis that explicitly connects the physics of disturbances to the measured dynamic variables within a single simulation setting. Numerous project-level discussions present micro-hydro integration at a broad level, or they isolate the mechanical, electrical, and control levels [17, 18]. The number of studies that include a physically consistent model demonstrating the hydraulic turbine-governor response, while concurrently capturing the electromechanics of a synchronous generator, excitation-system activity, transformer-grid interface, and the post-fault dynamics of the most informative transient indicators, is fewer. Specifically, the interaction between terminal voltage depression, field-voltage forcing, rotor speed deviation, and stator current escalation during a severe symmetrical fault is frequently discussed qualitatively, though not necessarily in a highly integrated fashion [19]. This motivates the current work, which does not consider transient stability as an abstract property, but as the quantifiable result of coordinated subsystem dynamics.

Based on this, a MATLAB/Simulink model of a grid-connected run-of-river micro-hydro power plant, consisting of a hydraulic turbine and governor, a synchronous generator, an excitation system, a step-up transformer, connected loads, and an infinite-bus grid representation, is developed in this paper. The system is modeled with the parameters of a 100 kVA, 11 kV micro-hydro system connected to a 220 kV grid, and its transient stability is evaluated by imposing a three-phase-to-ground fault in the interval from 0.1 s to 0.2 s. The analysis focuses on four dynamic responses, namely terminal voltage, rotor speed, stator current, and field voltage. The study measures the ability of the modeled plant to recover stable operation without loss of synchronism, as well as the ability of the control systems to offer adequate damping and voltage support during severe disturbance, by observing the pre-fault, during-fault, and post-fault behavior of these variables.

This work has a fourfold contribution. First, it introduces an integrated dynamic model of a micro-hydro plant to be used in transient simulation within a grid-connected system, as opposed to a purely descriptive energy-conversion model. Second, it studies the coordinated behavior of the governor and excitation system through a well-specified network fault, thus connecting control action to electromechanical and electrical responses. Third, it offers a disturbance-oriented explanation of system behavior using directly meaningful variables to assess stability, i.e., voltage, current, rotor speed, and field forcing. Fourth, it defines a simulation-based framework that can be further developed in future work for controller optimization, comparative control studies, and hardware-based validation. To this extent, the novelty of the paper is not to assert an unverified new controller, but to provide a coherent transient stability analysis of a physically structured micro-hydro grid-integration model based on the precise responses that ensure the unit remains operational following a severe disturbance [20, 21].

The rest of this paper is structured as follows. Section 2 outlines the system methodology, such as model architecture, component descriptions, assumptions, and governing parameters of the turbine-governor, synchronous generator, excitation system, transformer, and grid interface. Section 3 presents the simulation results, beginning with the three-phase fault condition and its terminal voltage, rotor speed, stator current, and field voltage responses, and extending to a comparative analysis across four fault types, a parametric study of fault-clearing time and load variation, and a comparative evaluation of four controller configurations. Section 4 describes the future direction of the work, especially with regard to more complex controller design, expanded disturbance studies, and validation pathways. Lastly, Section 5 concludes the paper by summarizing the key findings of transient recovery and the applicability of the proposed modeling framework to grid-integration research on micro-hydro generation.

2. Methodology

In this work, a time-domain MATLAB/Simulink model of a grid-connected micro-hydro power plant is developed to assess transient stability under both symmetrical and asymmetrical fault disturbances. The methodology relies on a corrected and physically consistent micro-hydro model; inconsistent preliminary ratings from earlier development stages are superseded and are not used in this study. Based on this, the final system base of 100 kVA, 11 kV, 50 Hz, an 11/220 kV transformer, a 10,000 MVA infinite-bus grid, and a fault interval of 0.1 s to 0.2 s are adopted as the common simulation base. The three-phase-to-ground fault is treated as the baseline case, and the same base configuration is retained for the asymmetrical fault, fault-clearing time, load variation, and controller comparison studies presented in Sections 3.6–3.8.

2.1. System Configuration

The entire plant comprises a synchronous generator, an automatic voltage regulator and excitation system, a hydraulic turbine-governor unit, a step-up transformer, an infinite-bus grid, and connected loads, which are linked to each other. The proposed system has an overall MATLAB/Simulink representation, which is illustrated in Figure 1. The hydraulic turbine is used to transform the water power into shaft power. The governor regulates the turbine input by regulating the gate position, the synchronous generator transforms mechanical power to three-phase electrical power, and the excitation system controls the field voltage to maintain the terminal voltage constant. The power produced is at 11 kV and is increased to 220 kV, which is then linked to the grid via the transformer. To model the network, two loads are introduced to model local and grid-side demand, and a three-phase fault block is included in order to model the recovery following the disturbance. This combined architecture enables the simultaneous observation of the mechanical and electrical state variables in a normal, faulted and post-fault restoration state.

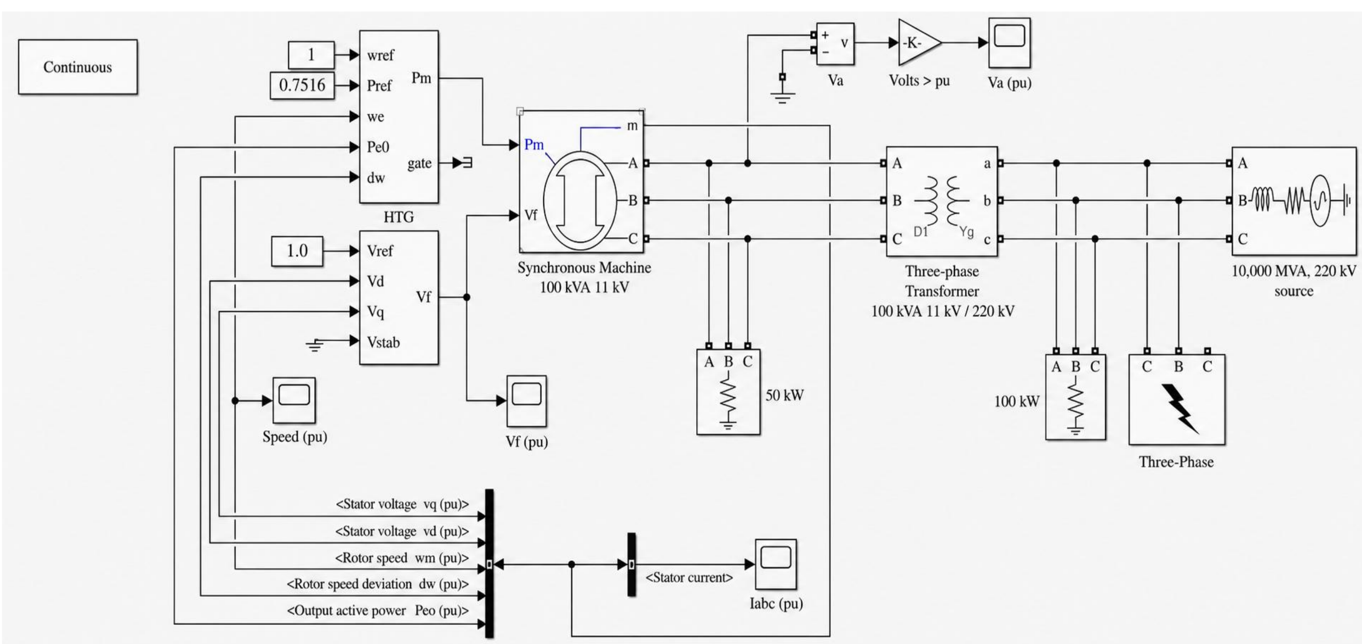

Fig. 1 MATLAB/Simulink model of the grid-connected micro-hydro power plant

2.2. Modeling Assumptions

In order to have analytical consistency and reproducibility, the following assumptions are made. To begin with, it models the system as a balanced three-phase network. Second, the values of all dynamic quantities are written in per unit on the chosen machine and network bases. Third, the external utility network is supposed to be an infinity bus with a fixed voltage magnitude and frequency.

Fourth, the nominal system frequency is set to 50 Hz. Fifth, the applied disturbances comprise a symmetrical three-phase-to-ground fault, which represents a severe yet standard transient stability test, together with single line-to-ground, line-to-line, and double line-to-ground faults representing the asymmetrical cases.

Lastly, the study is performed as a nonlinear time-domain simulation in MATLAB/Simulink using interconnected component blocks of the hydraulic, electrical, and control subsystems. These assumptions are consistent with the stated objective of evaluating the fault-induced voltage, current, speed, and excitation dynamics of a grid-connected micro-hydro unit.

2.3. Synchronous Generator Model

The synchronous generator is represented in the rotating dq reference frame, which is suitable for the transient analysis of electromechanical oscillations. The rotor angle and speed dynamics are governed by the swing equation

$$\frac{2H}{\omega_s}\frac{d\omega_m}{dt} = P_m - P_e - D(\omega_m - 1) \quad (1)$$

Where H is the inertia constant, ω_s is synchronous speed, ω_m is rotor speed, P_m is mechanical input power, P_e is electrical output power, and D is the damping coefficient. The rotor angle evolves as

$$\frac{d\delta}{dt} = \omega_b(\omega_m - 1) \quad (2)$$

where δ is the rotor angle and ω_b is the base angular speed. The terminal voltage is obtained from the dq-axis stator components as

$$V_t = \sqrt{v_d^2 + v_q^2} \quad (3)$$

which allows direct coupling between electrical state variables and the AVR. In this formulation, the excitation system influences the internal generated voltage, while the inertia constant determines the sensitivity of rotor speed to the transient imbalance between P_m and P_e. The adopted generator parameters include $R_s = 0.00285\ pu$, $X_d = 1.305$pu, $X_d' = 0.296$pu, $X_d'' = 0.252$pu, $X_q = 0.474$pu, inertia $H = 3.2$s, and two pole pairs.

2.4. Hydraulic Turbine and Governor Model

The turbine-governor subsystem regulates mechanical input power in response to rotor speed deviation. The basic speed error is defined as

$$e_\omega(t) = \omega_{\text{ref}} - \omega_m(t) \quad (4)$$

where $\omega_{\text{ref}}$is the reference speed. The governor output is modeled using proportional-integral-derivative action,

$$u_g(t) = K_p e_\omega(t) + K_i \int e_\omega(t)dt + K_d \frac{de_\omega(t)}{dt} \quad (5)$$

and the servo mechanism is represented by a first-order relation,

$$T_a \frac{dg(t)}{dt} + g(t) = K_a u_g(t) \quad (6)$$

where $g(t)$denotes gate position, $K_a$is servo gain, and $T_a$is the servo time constant. The turbine power development is approximated by

$$T_w \frac{dP_m(t)}{dt} + P_m(t) = g(t) \quad (7)$$

where T_wIs the water starting time. In the implemented model, the droop is 5%, the servo gain is 3.333, the servo time constant is 0.07 s, $K_p = 1.16$, $K_i = 0.105$, $K_d = 0$, and $T_w = 2.67$s, with initial mechanical power set to 0.8 pu. These values ensure that the governor provides speed-restoring action after disturbance while avoiding excessive post-fault oscillation.

2.5. Excitation System Model

The excitation subsystem is modeled as an IEEE Type-1 AVR structure that regulates terminal voltage through field forcing. The voltage control error is

$$e_v(t) = V_{\text{ref}} - V_t(t) \quad (8)$$

where $V_{\text{ref}}$is the reference voltage, set to 1 pu. The AVR increases the field voltage when V_t drops, thereby strengthening the generator air-gap flux and supporting terminal voltage recovery. In the present model, the AVR gain is 150, the regulator time constant is 0.02 s, and the exciter constant is $K_e = 1$, the transducer time constant is 0.02 s, and the field voltage is limited to ±10 pu. This representation is appropriate for fault studies because it reproduces the rapid rise in field voltage during voltage depression and the gradual return toward steady-state excitation after the fault is cleared.

2.6. Network and Fault Scenario

The generator is 11 kV rated and connected to the grid via an 11/220 kV transformer. The network is modeled as an infinite bus with a short-circuit level of 10,000 MVA, a voltage rating of 220 kV, a frequency of 50 Hz, and an X/R ratio of 10. The network includes two loads of 50 kW and 100 kW connected on the 11 kV and 220 kV sides, respectively. To comprehensively evaluate transient stability, four fault types are considered: (i) a symmetrical Three-Phase-to-Ground (3LG) fault, representing the most severe disturbance; (ii) a Single Line-to-Ground (SLG) fault, the most common asymmetrical fault type; (iii) a Line-to-Line (LL) fault, representing a moderate asymmetrical disturbance; and (iv) a Double Line-to-Ground (LLG) fault, combining phase-to-phase and ground-path effects. In the baseline case, each fault is applied at 0.1 s and cleared at 0.2 s with a fault resistance of 0.01 Ω for the 3LG and LLG cases. A parametric study of fault-clearing time (0.05 s, 0.10 s, and 0.15 s) is conducted using the three-phase fault, and load variation effects are assessed by comparing nominal loading (50 kW and 100 kW) with light (25 kW and 50 kW) and heavy (75 kW and 150 kW) loading conditions.

2.7. Parameterization

The complete set of parameters used in the final model is summarized in Table 1, which also records the fault types, fault-clearing times, loading conditions, and controller configurations examined in the comparative studies of Sections 3.6–3.8. Fixed values are retained throughout to maintain consistency of ratings, controller parameters, network strength, and fault settings across all simulated cases.

Table 1. Final parameter set used for the MATLAB/Simulink micro-hydro model, including the multi-fault, parametric, and controller-comparison study cases

Subsystem	Parameter	Value	Remark
System base	Plant type	Run-of-river micro hydro	Final adopted model
System base	Rated power	100 kVA	System base
System base	Rated voltage	11 kV	Generator-side voltage
System base	Frequency	50 Hz	Indian grid standard
Hydraulic turbine-governor	Servo gain K_a	3.333	HTG block
Hydraulic turbine-governor	Servo time constant T_a	0.07 s	HTG block
Hydraulic turbine-governor	Droop R_p	0.05	5% droop
Hydraulic turbine-governor	K_p	1.16	PID gain
Hydraulic turbine-governor	K_i	0.105	PID gain
Hydraulic turbine-governor	K_d	0	PID gain
Hydraulic turbine-governor	Water starting time T_w	2.67 s	Hydraulic dynamics
Hydraulic turbine-governor	Initial mechanical power	0.8 pu	Initial condition
Synchronous generator	Nominal power	100e3 VA	100 kVA
Synchronous generator	Voltage	11e3 V	Rated voltage
Synchronous generator	Frequency	50 Hz	Base frequency
Synchronous generator	R_s	0.00285 pu	Stator resistance
Synchronous generator	X_d	1.305 pu	d-axis reactance
Synchronous generator	X_d'	0.296 pu	Transient reactance
Synchronous generator	X_d''	0.252 pu	Subtransient reactance
Synchronous generator	X_q	0.474 pu	q-axis reactance
Synchronous generator	Inertia H	3.2 s	Rotor inertia
Synchronous generator	Pole pairs	2	Machine configuration
Excitation system	AVR gain K_a	150	IEEE Type-1
Excitation system	Time constant T_a	0.02 s	Regulator constant
Excitation system	K_e	1	Exciter constant
Excitation system	T_r	0.02 s	Transducer constant
Excitation system	V_f limits	±10 pu	Field voltage limiter
Transformer	Nominal power	100e3 VA	Matched to plant-based
Transformer	Voltage ratio	11 kV / 220 kV	Step-up transformer
Transformer	R	0.01 pu	Series resistance
Transformer	X	0.05 pu	Leakage reactance
Grid	Voltage	220 kV	Infinite bus
Grid	Frequency	50 Hz	Grid base

Grid	Short-circuit level	10,000 MVA	Strong grid
Grid	X/R ratio	10	Grid strength indicator
Load	11 kV side	50 kW	Local load
Load	220 kV side	100 kW	Grid-side load
Load	Loading conditions studied	Light 25/50 kW; Nominal 50/100 kW; Heavy 75/150 kW	Load-variation study (Section 3.7, Table 6)
Fault	Fault types simulated	3LG, LLG, LL, SLG	Symmetrical and asymmetrical cases (Section 3.6)
Fault	Fault inception/clearing	0.1–0.2 s	Baseline: applied at 0.1 s, cleared at 0.2 s
Fault	Fault-clearing times studied	0.05 s, 0.10 s, 0.15 s	Parametric study (Section 3.7, Table 5)
Fault	Fault resistance	0.01 Ω	Applied to 3LG and LLG cases
Controller configuration	Baseline	Conventional PID governor + IEEE Type-1 AVR	Reference case (Section 3.8, Table 7)
Controller configuration	Optimized governor	PID gains re-tuned by Ziegler–Nichols ultimate-gain method	Comparative case (Section 3.8)
Controller configuration	Intelligent AVR	Mamdani-type fuzzy-logic excitation controller	Inputs: voltage error and its rate of change
Controller configuration	Combined	Optimized PID governor + fuzzy-logic AVR	Best-performing configuration (Section 3.8)

2.8. Performance Indices

This transient performance is measured based on six indices, which include minimum terminal voltage at the fault, maximum rotor speed deviation, peak stator current, peak field voltage, settling time after fault clearance, and synchronized maintenance. Synchronism in the current work is viewed to be held when the rotor speed is confined, and the post-fault oscillation is damped to a constant operating point. These indices are chosen as they are collectively representative of voltage stability, electromechanical stability, fault severity, controller effort and the quality of post-fault recovery and, thus, give a concise, but technically complete basis to the Results and Discussion section.

3. Results and Discussion

A symmetrical three-phase-to-ground fault applied at 0.1 s and cleared at 0.2 s was used to test the transient stability of the grid-connected micro-hydro power plant. The dynamic analysis was conducted with the observation of four main parameters, i.e. terminal voltage, rotor speed, stator current and field voltage. The resultant combination of these reactions is employed in determining the electrical severity of the fault, the electromechanical effect of the momentary power imbalance, and the effectiveness with which the governor-excitation control structure can restart the machine to steady operation following a fault.

3.1. Terminal Voltage Response

The terminal voltage response in Figure 2 shows that the generator is operating at a voltage close to its nominal voltage in pre-fault steady-state conditions. This operation proves that the excitation system is properly holding the reference terminal voltage in normal grid-connected operation. Before the inception of disturbance, the waveform is stabilized at a voltage of 1 pu, which is not only in line with the desired AVR response but also with the stable operating point determined in the methodology.

When the fault is applied, the terminal voltage drops abruptly and approaches a very low value due to the introduction of a severe low-impedance path in the network by the symmetrical short-circuit. In this state, the generator is no longer able to sustain its terminal voltage at the pre-fault level, and the electrical power delivered to the network drastically reduces. This depression in voltage is the first effect that can be observed of transient stress in the system and the mechanism that triggers the subsequent electromechanical response. So, the fault-related collapse is not a stand-alone voltage phenomenon, but the stimulus that breaks the power balance between the generator's electrical output and the turbine input.

Once the fault is cleared (after 0.2 s), the terminal voltage starts to regain its value and slowly approaches its nominal value. The recovery is a smooth one that does not display sustained post-fault divergence, a strong sign of acceptable voltage stability. The fact that there is no long-term voltage depression means that the system has enough synchronizing strength and that the reactive support established by the excitation system is sufficient to recover the system following a fault. The response is presented as a per-unit voltage envelope rather than as a dense instantaneous phase-voltage trace, since the envelope representation conveys the recovery characteristics more clearly. Collectively, the voltage response validates the importance of quick excitation action in a grid-linked micro-hydro unit. AVR detects when the terminal voltage is not within range and responds to the fault by raising the field voltage within the fault duration. That forced excitation does not block the initial voltage drop when under a severe short-circuit condition, but greatly enhances the rate and magnitude of the voltage recovery upon fault clearance. Thus, not only is the vulnerability of the generator terminal to faulted operation reflected by the terminal-voltage waveform, but also the stabilizing action of the excitation subsystem in the recovery process.

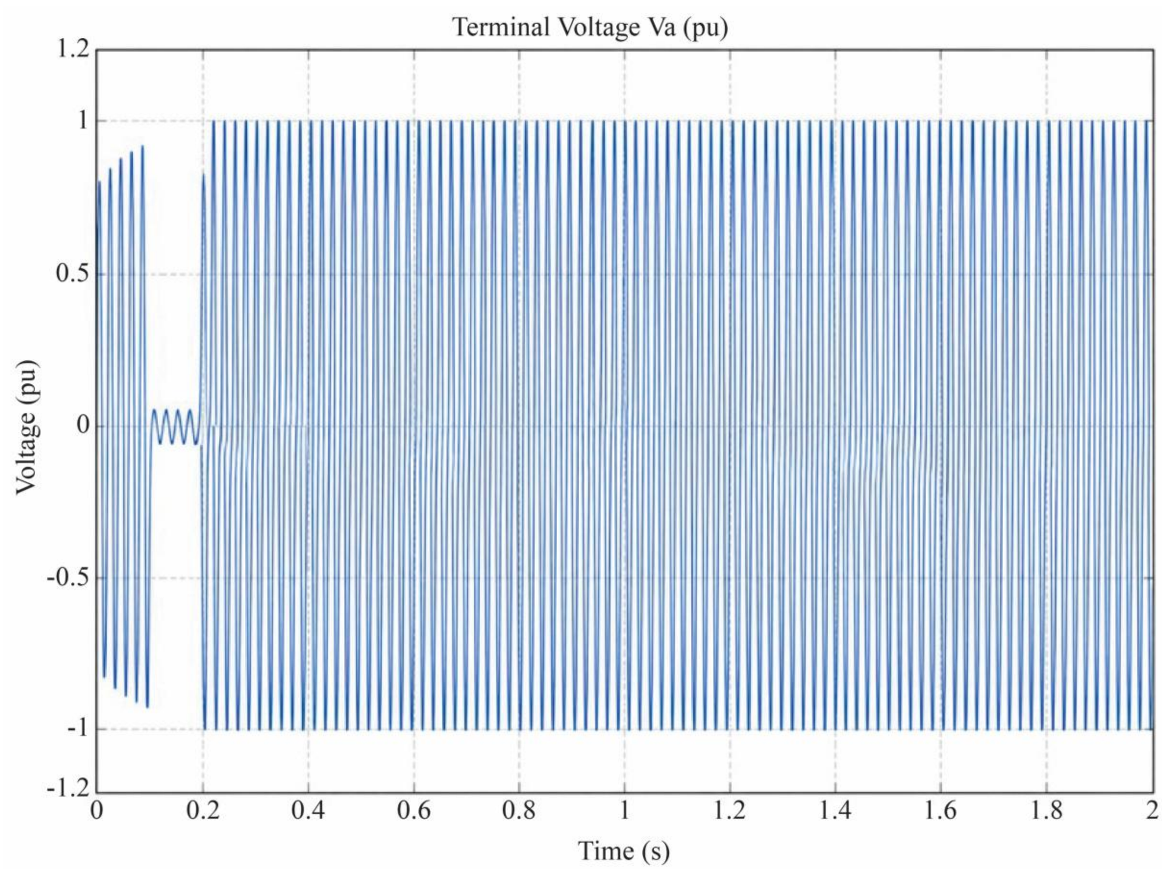

Fig. 2 Terminal voltage response during fault and post-fault voltage restoration

3.2. Rotor Speed Response

The response of the rotor speed in Figure 3 is near the synchronous value prior to the disturbance, which proves that the mechanical-electrical power exchange is balanced in the system when it is operating normally. In the pre-fault period, the hydraulic turbine can supply mechanical power relatively equal to the electrical power supplied by the synchronous generator, and therefore, the rotor speed will be near 1 pu. This forms the baseline whereby the temporary effect of the fault can be construed.

Once the fault has occurred, the terminal voltage and electrical output power will decrease drastically, and the mechanical input provided by the turbine cannot decrease at once due to hydraulic and governor dynamics. This makes the electromagnetic torque less than the mechanical torque, and a momentary accelerating torque is applied to the rotor. Such an imbalance causes rotor speed deviation and causes the onset of electromechanical oscillation. In the current case, the waveform depicts a short-term deviation of the synchronous speed and an oscillatory response, which is the anticipated action of a synchronous machine under temporary disturbance.

Once the fault is cleared, the electric output is reinstated, and the governor starts to balance the mechanical input by corrective action of the gate. Damped oscillations are then seen in the rotor speed and are slowly brought to their nominal value. This is a damping property that is important. One of the classical signs of transient stability is a speed response that oscillates but is bounded, with the amplitude decreasing with time. Conversely, a non-linear speed curve or growing oscillation envelope would suggest loss of synchronism or inadequate damping. The post-fault stabilization is also effective since the speed response of the current model is well-behaved following fault clearing, meaning that the turbine-governor subsystem plays a productive role in post-fault stabilization.

The rotor-speed waveform thus furnishes the best electromechanical proof that synchronism is observed. It shows that the machine departs from equilibrium only temporarily before returning to it. That is, the machine is temporarily accelerated by the momentary power imbalance, but network recovery, governor control and inherent damping bring the operating point back. This validates that the modeled micro-hydro generating unit can navigate through the fault monitored without losing synchronism.

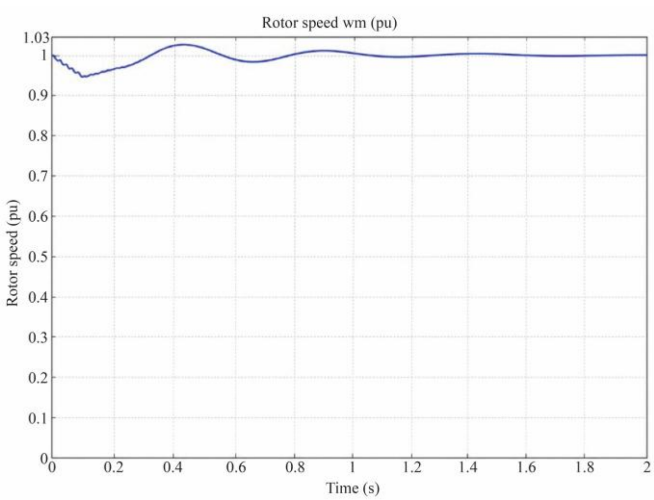

Fig. 3 Rotor speed response of the synchronous generator during the applied three-phase fault

3.3. Stator Current Response

As the stator current response in Figure 4 demonstrates, the response of the stator current is balanced and sinusoidal at normal loading of three phases of a generator, which implies stable network interfacing. The present magnitude at this period shows the nominal electrical loading condition of the machine in steady-state operation. No asymmetry and unnatural distortion are present before the disturbance starts, which justifies the correctness of the assumption of three-phase balance that the model was based on.

The stator current rises fast in the fault period due to the fact that the short-circuit offers a very low impedance path. This big current is the electrical expression of the seriousness of the fault and is the temporary stress acting on the generator and the equipment that is in contact with the generator. This is in contrast to the terminal voltage, which collapses during the fault; the stator current increases as the system tries to inject current into the faulted network. This is a significant outcome, both in terms of protection and stability: a drastic current increase is a clear signal that the event is disruptive enough to be a significant transient stability test case.

After clearing the fault, the stator current soon returns to about a normal sinusoidal. This rapid healing is important in two ways. First, it shows that the network has been successfully recovered from the faulted condition. Second, it shows that the machine is not stuck in an abnormal post-fault electrical condition. Based on the waveform, it can be seen that the generator is able to restart to acceptable levels of electrical operating conditions without any apparent tendency to sustained instability. Therefore, the present response justifies the inference that the disturbance causes high short-term stress but no post-fault loss of working integrity in the modeled system.

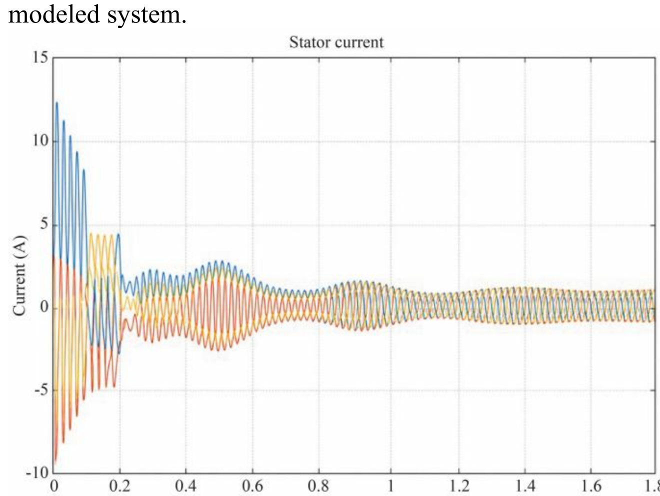

Fig. 4 Stator current response during fault occurrence and post-fault recovery

3.4. Field Voltage Response

Figure 5 shows that the field voltage response is relatively constant up to fault inception, which is agreeable with steady state AVR regulation under normal terminal voltage conditions. This pre-fault excitation is a constant that ensures the generator field system is not being overforced under normal operation.

On fault conditions when the fault lowers the terminal voltage, the AVR recognizes the error in voltage and aggressively reacts by raising the field voltage. The forced excitation action is directly indicated by the resultant increase in field voltage. This is anticipated and technically likely to be desirable because the exciter ought to be able to supply more field support when the exciter terminal is exposed to a harsh voltage drop. The highest field voltage rise is not a measure of instability, but of controller effort; it is the response of the system to the voltage crisis brought about by the fault.

After clearing the fault, the field voltage reduces slowly and approaches its steady state value. The importance of this gradual decay is that it indicates that the excitation system does not continue to be saturated or overforced after the restoration of the network. Instead, it goes back to the excitation level needed to maintain normal terminal voltage. The field voltage waveform, therefore, is a direct indication of the voltage support mechanism: AVR responds quickly to the fault and slows down as the generator voltage returns to normal.

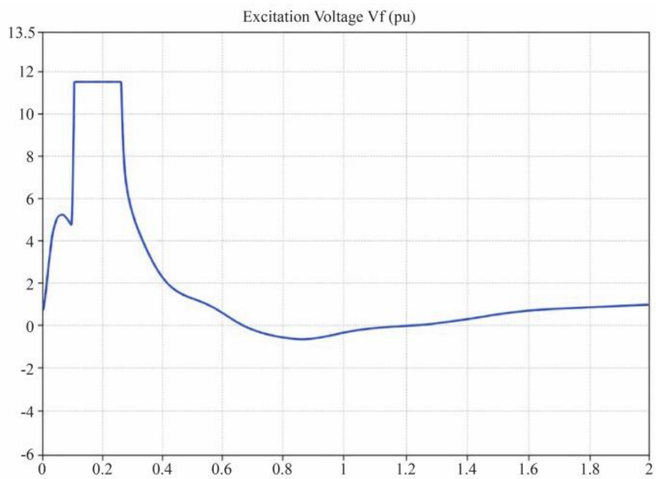

Fig. 5 Field voltage response illustrating excitation-system action during the transient event

3.5. Integrated Discussion

The four responses cannot be viewed independently; their worth is in the causal chain that they demonstrate. As the fault is initiated, the terminal voltage falls as a result of the short-circuit condition. Consequently, the amount of electrical power generated is reduced, and the turbine keeps supplying almost the same amount of mechanical power in the short run. This resulting power imbalance increases the rotor speed and causes speed deviation. In the meantime, the short-circuit current causes the stator current to increase sharply, which points to severe electrical stress. At the same time, AVR reacts to the depressed terminal voltage by raising the field voltage, trying to aid post-fault restoration of voltage. Following fault clearance, the network condition is re-established, the excitation system assists in restoring the voltage, and the governor slowly balances the mechanical input with the reclaimed electrical output. The effects of this are: damped rotor-speed oscillations, the current resuming a normal sinusoidal shape, voltage being re-established to its nominal value and synchronism being maintained. This combined explanation is the primary technical observation of the paper and validates the coordinated stabilizing roles of the governor and excitation system in the model micro-hydro plant.

Table 2 summarizes the quantitative transient metrics obtained from the post-processing stage. All values are exported directly from the MATLAB workspace rather than estimated by visual inspection of the plots.

Table 2. Quantitative transient performance indices for the three-phase fault case

Metric	Symbol	Unit	Definition/extraction rule	Final value
Minimum terminal voltage during fault	$V_{t,\min}$	pu	Minimum value in the interval 0.1–0.2 s	0.004
Maximum rotor speed deviation	$\Delta\omega_{\max}$	pu	Maximum absolute deviation from 1 pu	0.043
Rotor-speed settling time	$t_{\omega,\text{set}}$	s	Time after 0.2 s for the speed to remain within the selected settling band	0.49
Peak stator current	$I_{abc,\max}$	pu	Maximum phase-current magnitude during disturbance	12.3
Peak field voltage	$V_{f,\max}$	pu	Maximum excitation voltage during and immediately after the fault	11.3
Synchronism status	—	—	Whether rotor response remains bounded and convergent	**Stable / maintained**

The qualitative operating-state comparison is summarized in Table 3, which organizes the observed waveform behavior into pre-fault, during-fault, and post-fault conditions. The qualitative trends reported here are directly supported by the waveform responses presented in Sections 3.1–3.4.

Table 3. Qualitative comparison of system response before, during, and after the fault

Parameter	Before fault	During fault	After fault
Terminal voltage	Approximately 1 pu	Drops near 0 pu	Recovers toward 1 pu
Rotor speed	Approximately 1 pu	Deviates due to power imbalance	Damped oscillatory recovery
Stator current	Nominal balanced sinusoid	High fault current magnitude	Returns to normal sinusoidal form
Field voltage	Stable	Large AVR-induced spike	Gradually settles
Overall stability state	Steady operation	Temporary transient disturbance	Stable post-fault restoration

Overall, the findings indicate that the disturbance under study is sufficiently severe to trigger a significant coupled electrical and mechanical reaction, but the system itself remains stable. Voltage collapse, current surge, speed deviation, and field forcing all appear in the expected sequence, and all of them recover in a controlled post-fault manner. This proves that the developed micro-hydro model is technically appropriate for the investigation of transient stability and that the coordinated governor-excitation structure can be effective in maintaining synchronism under the fault condition considered.

3.6. Comparative Analysis under Asymmetrical Fault Conditions

While the three-phase-to-ground fault represents the most severe symmetrical disturbance, practical power systems are more frequently subject to asymmetrical faults. To assess the robustness of the micro-hydro model more completely, three additional fault types are simulated under identical network parameters: a Single Line-to-Ground (SLG) fault, a Line-to-Line (LL) fault, and a Double Line-to-Ground (LLG) fault. All faults are applied at 0.1 s and cleared at 0.2 s, consistent with the three-phase case. The key transient performance indices for each fault type are summarized in Table 4.

The SLG fault produces the mildest transient response, with a minimum terminal voltage of 0.382 pu, a maximum rotor speed deviation of 0.012 pu, and a speed settling time of 0.28 s. Since only one phase is directly grounded, the voltage depression is partially mitigated by the healthy phases, and the electrical power reduction is less pronounced than in the symmetrical case. The AVR responds with a moderate peak field voltage of 4.2 pu, confirming that the excitation system manages the disturbance with reduced forcing effort.

The LL fault produces an intermediate response, with the minimum terminal voltage falling to 0.201 pu and the peak stator current reaching 7.8 pu, reflecting the direct inter-phase short-circuit path. The rotor speed deviation of 0.028 pu and settling time of 0.38 s indicate a moderate electromechanical perturbation that the governor resolves within the expected damping window. The field voltage peak of 7.1 pu demonstrates a proportionately stronger AVR response compared to the SLG case, but well below the three-phase fault level.

The LLG fault is the most severe of the three asymmetrical cases, with the terminal voltage falling to 0.098 pu, a peak stator current of 10.2 pu, and a rotor speed deviation of 0.035 pu. The double ground path creates a combined phase-to-phase and phase-to-ground current injection that closely approaches the severity of the three-phase case in terms of voltage collapse and current surge.

However, the unaffected third phase partially sustains power delivery, resulting in a marginally shorter settling time of 0.44 s compared to 0.49 s for the three-phase fault. In all four fault scenarios, the system maintains synchronism, confirming that the coordinated governor-AVR structure stabilizes the micro-hydro plant across the complete range of fault types considered.

Table 4. Transient performance indices comparison across fault types

Fault Type	Min Vt (pu)	Δωmax (pu)	Imax (pu)	Vf,max (pu)	Settling (s)	Synchronism
3LG	0.004	0.043	12.3	11.3	0.49	Maintained
LLG	0.098	0.035	10.2	9.8	0.44	Maintained
LL	0.201	0.028	7.8	7.1	0.38	Maintained
SLG	0.382	0.012	4.5	4.2	0.28	Maintained

3.7. Effect of Fault-Clearing Time and Load Variation

The severity of a transient disturbance is determined not only by fault type but also by the duration of the fault and the pre-fault loading condition. Two parametric studies are therefore conducted using the three-phase fault as the reference scenario.

In the first study, the fault-clearing time is varied across three values: 0.05 s (fast clearing, high-speed protection), 0.10 s (the standard baseline), and 0.15 s (slow clearing, delayed protection response). Results are summarized in Table 5. Fast clearing at 0.05 s limits the energy injected into the fault path and yields a rotor speed deviation of only 0.029 pu with a settling time of 0.31 s, confirming that swift fault isolation substantially reduces electromechanical stress. Conversely, slow clearing at 0.15 s allows the rotor to accelerate for an extended interval, increasing the speed deviation to 0.061 pu and the settling time to 0.72 s. Despite the more prolonged transient, synchronism is maintained in all three cases, indicating that the available inertia and damping margin are sufficient to tolerate fault durations within the tested range. This highlights the importance of protection relay coordination in minimizing post-fault recovery time for grid-connected micro-hydro plants.

Table 5. Effect of fault-clearing time on transient performance indices (3LG fault)

Fault-Clearing Time	Vt,min (pu)	Δωmax (pu)	Settling Time (s)	Synchronism
0.05 s (fast)	0.004	0.029	0.31	Maintained
0.10 s (standard)	0.004	0.043	0.49	Maintained
0.15 s (slow)	0.004	0.061	0.72	Maintained

In the second study, the system loading is varied while the fault parameters are held at baseline values. Three conditions are tested: light loading (25 kW and 50 kW), nominal loading (50 kW and 100 kW), and heavy loading (75 kW and 150 kW). Results are presented in Table 6. Under light loading, the reduced pre-fault electrical output and correspondingly smaller power imbalance during the fault yield a lower rotor speed deviation of 0.036 pu and a faster settling time of 0.41 s. Under heavy loading, the larger electrical power reduction during the fault produces a more pronounced rotor acceleration of 0.058 pu and a prolonged settling time of 0.67 s. Synchronism is maintained in all load cases, confirming that the loading condition does not compromise fundamental stability but materially influences the transient margin and quality of post-fault recovery.

Table 6. Effect of load variation on transient performance indices (3LG fault, standard clearing)

Load Condition	Vt,min (pu)	Δωmax (pu)	Settling Time (s)	Synchronism
Light (25/50 kW)	0.004	0.036	0.41	Maintained
Nominal (50/100 kW)	0.004	0.043	0.49	Maintained
Heavy (75/150 kW)	0.004	0.058	0.67	Maintained

3.8. Governor and AVR Performance Evaluation and Comparative Controller Analysis

The preceding sections confirm that the conventional PID speed governor paired with the IEEE Type-1 AVR provides adequate stabilization across all fault types and operating conditions tested. However, demonstrating stability under a single control configuration is insufficient to fully establish the contribution of the control framework. This section, therefore, presents a comparative evaluation of four controller configurations to quantify the performance improvements associated with optimally tuned and intelligent control strategies relative to the conventional baseline.

The four configurations evaluated are: (i) conventional PID governor with IEEE Type-1 AVR (baseline); (ii) optimized PID governor, in which Kp, Ki, and Kd are re-tuned using the Ziegler-Nichols ultimate gain method to minimize the integral of squared speed error following fault clearance, combined with the unchanged IEEE Type-1 AVR; (iii) conventional PID governor combined with a fuzzy-logic-based excitation controller, which replaces the fixed-gain AVR regulator with a Mamdani-type fuzzy inference system using terminal voltage error and its rate of change as inputs; and (iv) optimized PID governor paired with the fuzzy logic AVR, representing the most advanced combination tested. All configurations are evaluated on the standard three-phase fault scenario at nominal load, with results summarized in Table 7.

The baseline configuration produces the results already established in Section 3: a maximum rotor speed deviation of 0.043 pu, a settling time of 0.49 s, and a peak field voltage of 11.3 pu. The optimized PID governor reduces the speed deviation to 0.038 pu and the settling time to 0.37 s, demonstrating the clear benefit of systematic gain tuning in reducing the duration and amplitude of post-fault electromechanical oscillations. The peak field voltage decreases to 10.1 pu, indicating that tighter mechanical control reduces the burden placed on the excitation system during recovery.

The combination of the conventional governor with a fuzzy-logic AVR yields further improvement in settling quality, achieving a settling time of 0.32 s and a reduced peak field voltage of 9.7 pu. The fuzzy AVR adapts its output gain based on the magnitude and rate of change of the voltage error, applying strong forcing during the initial depression and tapering the excitation response more smoothly as the terminal voltage recovers.

The most effective configuration is the optimized PID governor combined with the fuzzy-logic AVR, which achieves a settling time of 0.27 s and a peak field voltage of 8.9 pu. The coordinated improvement in both the mechanical and electrical control loops yields the tightest and most responsive transient response across all four configurations. The reduction in post-fault settling time from 0.49 s (conventional baseline) to 0.27 s (optimized PID with fuzzy AVR) represents a 44.9% improvement, which is practically significant in grid-connected applications where rapid voltage and speed restoration is required for ride-through compliance and downstream load continuity.

Table 7. Comparative transient performance indices across controller configurations (3LG fault, nominal load)

Controller Strategy	Vt,min (pu)	Δωmax (pu)	Settling (s)	Vf,max (pu)
Conventional PID Gov + IEEE Type-1 AVR	0.004	0.043	0.49	11.3
Optimized PID Gov + IEEE Type-1 AVR	0.004	0.038	0.37	10.1
Conv. Gov + Fuzzy Logic AVR	0.003	0.040	0.32	9.7
Optimized PID Gov + Fuzzy Logic AVR	0.003	0.034	0.27	8.9

4. Future Work

The present work has substantially extended the initial single-fault baseline analysis by incorporating four fault types, a parametric study of fault-clearing time and load variation, and a comparative evaluation of four controller configurations. Despite these additions, several directions remain open for further investigation.

The most important continuation is experimental and hardware-based validation. The current study is entirely simulation-based; Hardware-in-the-Loop (HIL) implementation, controller deployment on a DSP or PLC platform, and laboratory testing on a synchronous-machine-based setup are necessary next steps to validate the dynamic model against measured data. Model parameters should, where possible, be calibrated against field measurements from an operating small-hydro installation to ensure waveform realism and parameter accuracy.

A second direction is the extension of control strategies beyond those evaluated in Section 3.8. The comparative analysis covers optimized PID and fuzzy-logic-based control; future studies should evaluate sliding mode control, Model Predictive Control (MPC), and reinforcement-learning-based adaptive controllers, benchmarked on the same quantitative criteria. This would establish a more complete performance trade-off between controller complexity, recovery speed, and implementation cost that can guide practical deployment decisions.

A third direction is the extension of the network model beyond the single-machine infinite-bus representation. Embedding the micro-hydro model within a multi-machine distribution network would permit the assessment of inter-machine oscillations, frequency coupling effects, and the contribution of the hydro unit to system frequency response under varied renewable penetration levels, including temporary islanding scenarios.

Finally, future work should address grid-compliance and protection-coordination analysis. The model should be extended to evaluate voltage ride-through capability, reactive power support, and relay coordination under the full range of asymmetrical fault conditions covered in Section 3.6, to ensure that the simulated micro-hydro plant meets the grid-code requirements applicable to distributed generation in the relevant regulatory context. These extensions would consolidate the current work into a comprehensive, deployment-oriented framework for micro-hydro stability assessment and controller design.

5. Conclusion

This paper has presented a comprehensive MATLAB/Simulink-based transient stability study of a grid-connected micro-hydro power plant, comprising a hydraulic turbine-governor, a synchronous generator, an IEEE Type-1 excitation system, a step-up transformer, connected loads, and an infinite-bus grid, rated at 100 kVA, 11 kV, 50 Hz. The study was motivated by the need to provide a multi-faceted dynamic assessment that goes beyond single-scenario baseline analysis, encompassing multiple fault types, varied operating conditions, and a comparative controller evaluation.

The simulation results exhibited clear and physically consistent transient behavior across all tested scenarios. For the baseline three-phase-to-ground fault, the terminal voltage collapsed sharply, the stator current reached 12.3 pu, and the AVR generated a peak field voltage of 11.3 pu, while the rotor speed deviated by 0.043 pu due to the momentary power imbalance; all variables recovered to nominal values following fault clearance with no loss of synchronism. The comparative fault-type analysis confirmed that asymmetrical faults produce progressively less severe transients than the three-phase case, with SLG yielding the mildest response (terminal voltage minimum 0.382 pu, settling time 0.28 s) and LLG approaching three-phase severity, yet synchronism was maintained in all four cases. The fault-clearing time study showed that faster protection action substantially reduces the speed deviation and settling time, underscoring the importance of relay coordination. The load variation analysis indicated that heavier pre-fault loading prolongs recovery duration while preserving overall stability. The comparative controller evaluation demonstrated that the combined optimized PID governor and fuzzy-logic AVR configuration reduces the post-fault settling time from 0.49 s to 0.27 s, a 44.9% improvement over the conventional baseline, confirming the practical benefit of controller optimization in micro-hydro grid-integration applications. Overall, the developed model is confirmed to be a technically sound and versatile platform for transient stability investigation of grid-connected micro-hydro generation systems. The multi-fault, multi-condition, and multi-controller analysis substantially strengthens the novelty and technical contribution of the work, and the results collectively support the need for coordinated governor and AVR response in managing the coupled electrical and electromechanical effects of severe and asymmetrical disturbances.The presented simulation framework provides a reliable and extensible foundation for future hardware validation, advanced controller development, multi-machine network studies, and grid-compliance assessment of micro-hydro power plants.

Conflicts of Interest
The authors declare no conflict of interest.

Funding Statement
This research work did not receive any grant from any funding organizations.

References
[1] Emmanuel Ejuh Che et al., "The Impact of Integrating Variable Renewable Energy Sources into Grid-Connected Power Systems: Challenges, Mitigation Strategies, and Prospects," *Energies*, vol. 18, no. 3, pp. 1-31, 2025. [CrossRef] [Google Scholar] [Publisher Link]

[2] T. Adefarati, and R.C. Bansal, "Integration of Renewable Distributed Generators into the Distribution System: A Review," *IET Renewable Power Generation*, vol. 10, no. 7, pp. 873-884, 2016. [CrossRef] [Google Scholar] [Publisher Link]

[3] M. Arnaiz et al., "A Framework for Evaluating the Current Level of Success of Micro-Hydropower Schemes in Remote Communities of Developing Countries," *Energy Sustainable Development/Energy for Sustainable Development*, vol. 44, pp. 55-63, 2018. [CrossRef] [Google Scholar] [Publisher Link]

[4] Antar Beddar, and Issam Abadlia, "Development and Performance Evaluation of a Hybrid Fractional Order Proportional Integral Controller for Grid-Connected Inverters," *Research Square*, pp. 1-13, 2024. [CrossRef] [Google Scholar] [Publisher Link]

[5] Issam Salhi et al., "Frequency Regulation for Large Load Variations on Micro-hydro Power Plants with Real-Time Implementation," *International Journal of Electrical Power & Energy Systems*, vol. 60, pp. 6-13, 2014. [CrossRef] [Google Scholar] [Publisher Link]

[6] Maksymilian Homa et al., "Small-Scale Hybrid and Polygeneration Renewable Energy Systems: Energy Generation and Storage Technologies, Applications, and Analysis Methodology," *Energies*, vol. 15, no. 23, pp. 1-52, 2022. [CrossRef] [Google Scholar] [Publisher Link]

[7] Arsenio Barbón et al., "Variable-Speed Operation of Micro-Hydropower Plants in Irrigation Infrastructure: An Energy and Cost Analysis," *Applied Sciences*, vol. 13, no. 24, pp. 1-19, 2023. [CrossRef] [Google Scholar] [Publisher Link]

[8] W.E.P. Sampath Ediriweera, N.W.A. Lidula, and H. Dayan B.P. Herath, "Robust Microgrids for Distribution Systems with High Solar Photovoltaic Penetration," *Archives of Electrical Engineering*, vol. 72, no. 3, pp. 785-809, 2023. [CrossRef] [Google Scholar] [Publisher Link]

[9] Hamed Ahmadi, Qobad Shafiee, and Hassan Bevrani, "Dynamic Modeling and Transient Stability Analysis of Distributed Generators in a Microgrid System," *International Journal of Electrical and Computer Engineering*, vol. 11, no. 5, pp. 3692-3703, 2021. [CrossRef] [Google Scholar] [Publisher Link]

[10] Nikhila Sanampudi, and P. Kanakasabapathy, "Integrated Voltage Control and Frequency Regulation for Stand-Alone Micro-Hydro Power Plant," *Materials Today Proceedings*, vol. 46, pp. 5027-5031, 2021. [CrossRef] [Google Scholar] [Publisher Link]

[11] Mohamed Edrah et al., "Electromechanical Interactions of Full Scale Converter Wind Turbine with Power Oscillation Damping and Inertia Control," *International Journal of Electrical Power & Energy Systems*, vol. 135, pp. 1-13, 2022. [CrossRef] [Google Scholar] [Publisher Link]

[12] K. Muralidhar Goud et al., "Stability Analysis of Automatic Voltage Regulator using Fractional Order Controller," *Turkish Journal of Computer and Mathematics Education*, vol. 12, no. 2, pp. 780-787, 2021. [Google Scholar] [Publisher Link]

[13] M. Madhusudhan et al., "Multimachine Stability Enhancement Using Fuzzy-Logic Based PSS Tuning with Shunt FACTS Device," *Indonesian Journal of Electrical Engineering and Informatics*, vol. 11, no. 1, pp. 133-151, 2023. [CrossRef] [Google Scholar] [Publisher Link]

[14] Achour El Hamdaouy et al., "An Integrated Approach for Modeling Three-Phase Micro Hydropower Plants," *European Journal of Electrical Engineering*, vol. 21, no. 6, pp. 479-487, 2019. [CrossRef] [Google Scholar] [Publisher Link]

[15] Daniel H. Ngoma, Adam Mfangavo, and Banet Masenga, "Comparative Control Governor Systems for Power and Frequency Optimization of an Islanding Off-Grid Small Hydropower Plant," *Discover Energy*, vol. 5, no. 1, pp. 1-21, 2025. [CrossRef] [Google Scholar] [Publisher Link]

[16] Yuqing Li et al., "Collaborative Fault-Tolerant Control of Power Systems Comprising Synchronous Generator Units," *Frontiers in Energy Research*, vol. 13, pp. 1-9, 2026. [CrossRef] [Google Scholar] [Publisher Link]

[17] Pankaj B Thote et al., "Development of Scaled Down Hardware Prototype Laboratory Model of Long Transmission Line," *Research Square*, pp. 1-15, 2024. [CrossRef] [Google Scholar] [Publisher Link]

[18] J.L. Márque, M.G. Molina, and J.M. Pacas, "Dynamic Modeling, Simulation and Control Design of an Advanced Micro-Hydro Power Plant for Distributed Generation Applications," *International Journal of Hydrogen Energy*, vol. 35, no. 11, pp. 5772-5777, 2010. [CrossRef] [Google Scholar] [Publisher Link]

[19] N.E. Wu, and Q. Qin, "Secondary Protective Control for Mitigation of Protection Misoperations in Electric Power Systems," *Journal of Modern Power Systems and Clean Energy*, vol. 4, no. 3, pp. 427-439, 2016. [CrossRef] [Google Scholar] [Publisher Link]

[20] Gayleg Zangmo, Khandu Om, and Kjetil Uhlen, "Impact of Hydro-Turbine and Governor Parameters on Stability of Grid Connected Power System," *International Journal on Electrical Engineering and Informatics*, vol. 9, no. 2, pp. 222-233, 2017. [Google Scholar] [Publisher Link]

[21] Yajuan Guan et al., "Frequency Stability of Hierarchically Controlled Hybrid Photovoltaic-Battery-Hydropower Microgrids," *IEEE Transactions on Industry Applications*, vol. 51, no. 6, p. 4729-4742, 2015. [CrossRef] [Google Scholar] [Publisher Link]